AOPAF: Arecibo Observatory Phased Array Feed

By Germán Cortés-Medellín
National Astronomy and Ionosphere Center
Cornell University
Sep 13, 2010

The Arecibo Footprint

An iconic feature of the Arecibo radio telescope is its Gregorian optics, hidden inside of the Gregorian dome, consisting of two shaped surfaces: the secondary and tertiary reflectors (see Figure 1). These reflectors are specially shaped to correct the spherical aberration produced by the (300m) main spherical reflector and concentrate the collected energy by the main reflector into the single focal point of the optics.
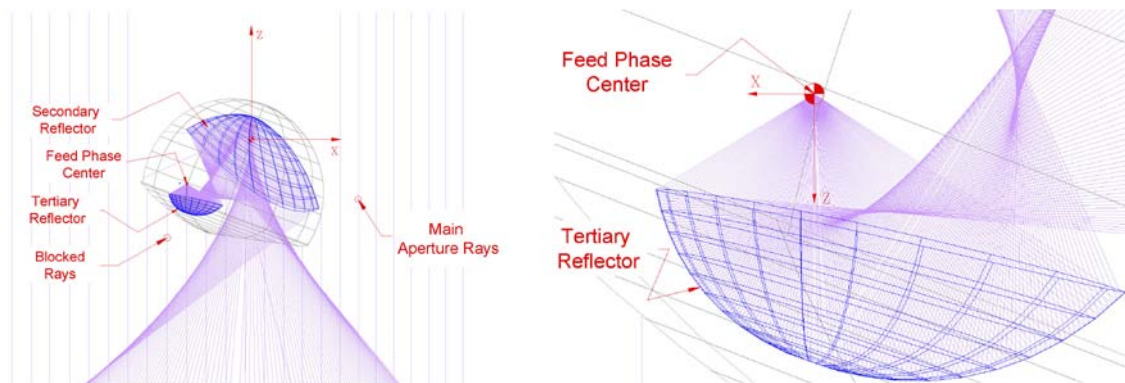

Figure 1. Left: Ray tracing of the secondary and tertiary reflectors of the Arecibo Gregorian Optics. Right: focal point detail after the tertiary reflector

In addition to correct the spherical aberration, the three-reflector Gregorian system produces a nearly uniformly illuminated elliptical aperture that yields aperture efficiencies of the order of 80%.

A single pixel L-Band (1.4 GHz) feed produces an elliptical beam of 200arcsec x 230arcsec in size in the sky (Figure 2, left). A seventh fold increase in survey speed was attained with the installation and operation of the 7-pixel L-Band camera: ALFA, in 2004. ALFA takes advantage of the large collecting area of the Arecibo telescope by observing simultaneously at 7 separate points in the sky. (Figure 2, center). The next logical step is to increase the survey speed by increasing further the number of simultaneous beams in the sky. An impression of a possible sky footprint of this new instrument is depicted right, in Figure 2, by an array with the equivalent of approximately 40 beams. As we will see later on, the figure of merit of interest is not the number of beams but rather the instantaneous FOV. The name of this new instrument is the Arecibo Observatory Phased Array Feed (AO PAF).
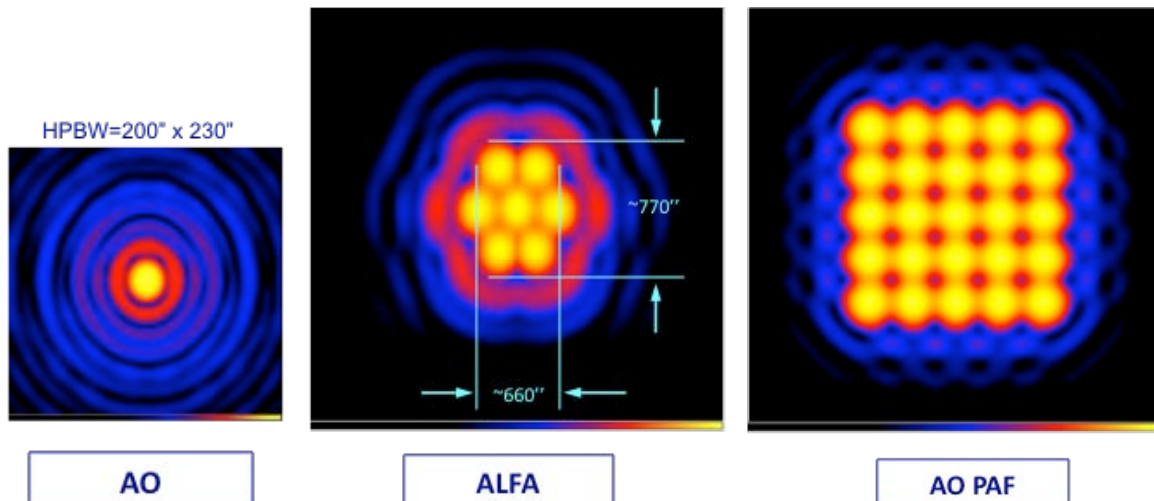
Figure 2. Comparison of the sky footprint of different AO instruments. Left: L-Band (1.4 GHz) single pixel beam pattern in the sky. Center: ALFA camera's 7-pixel beam footprint in the sky. Right: AO PAF (Arecibo Phased Array Feed) simulated sky footprint for a rectangular array configuration.

Available Field of View

While the AO shaped optics works remarkably well when the feed is located at the designed focus point, it losses efficiency rapidly when the feed is displaced from that ideal position. As the feed moves (scans) in the focal plane of the telescope optics, the corresponding beam moves in the sky by a given amount related to the plate scale of the optics.
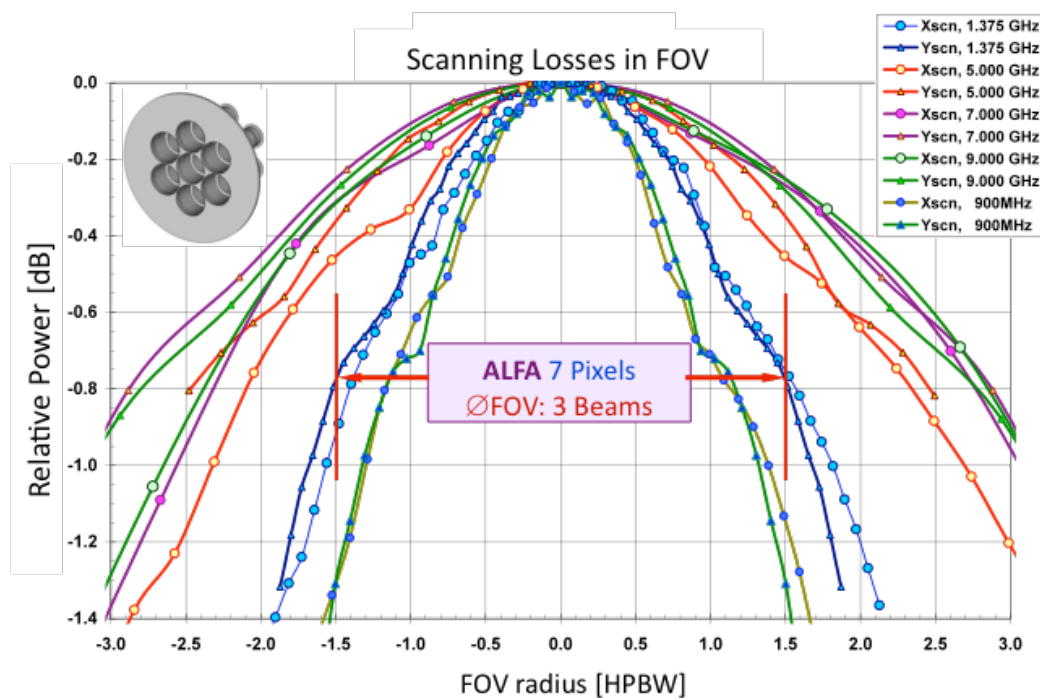

Figure 3. Scanning loss of the AO optics as a function of sky beam displacements

Figure 3 shows the scanning losses, for different frequencies, as a function of the corresponding sky beam displacement in beam widths. The figure shows in particular the regime of operation for ALFA, corresponding to a 3-beams across, at 1.375 GHz and at approximately 0.8 dB of scanning loss. At higher frequencies it is possible to accommodate more beams with the same scanning loss, i.e., at 9 GHz is 6 beams across.
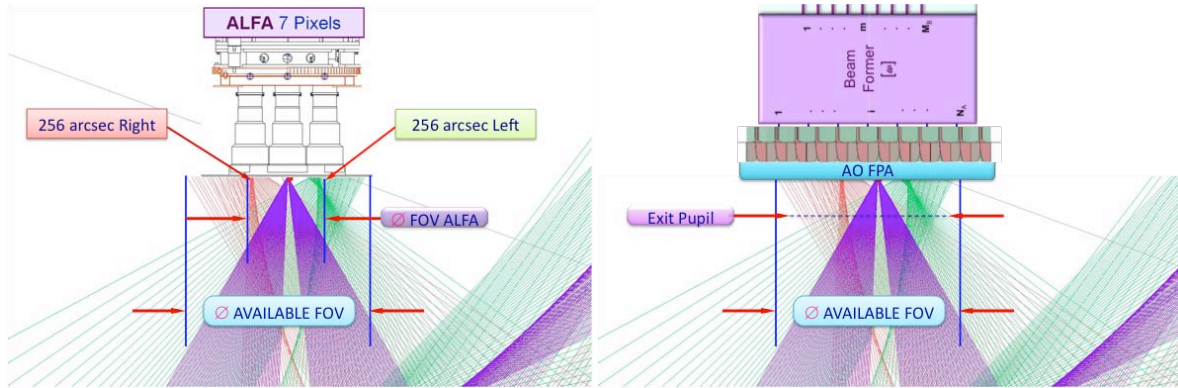

Figure 4. Ray tracing of the AO optics showing the caustics surfaces responsible mainly responsible for the scanning loss. In purple the beam is on axis, in red the beam is steered 256 arcsec to the right, in green, 256 arcsec to the left, respectively. Left: With ALFA. Right: Recovering the lost energy with a Phased Array Feed.

The reason behind the scanning loss is depicted more clearly in Figure 4 (left) which shows three different ray tracing bundles corresponding to receiving a plane wave (this equivalent to steering the beam in that particular direction) from a point source coming from three different directions in the sky: In purple, on axis, in red 256 arcsec to the right and in green 256 arcsec to the left. It is possible to see that all the energy will be collected by the central pixel of ALFA, but some of the energy misses the adjacent pixels lost in the caustics spreading. Using a Phased Array Feed (PAF), Figure 4 (right) it is possible to recover this energy back, hence increasing the telescope sensitivity over bigger instantaneous FOV. The largest FOV should be located close to the exit pupil of the telescope.

Phased Array Feed PAF

Figure 5 shows the basic principle of operation of a focal phased array feed. The PAF system consists of a front end and a beam former system back-end. The front end consists of a N_A number of antenna elements, each connected to a low noise amplifier. For noise control in an astronomical application, the LNA's and possibly the antenna elements will be cryogenically cooled.

In the beam former the signals of each of the N_A antenna elements is multiplied by a complex weighting factor and summed together. A particular set of weights (ω_m) produces a single m-beam in the FOV of the telescope. The total number of beams N_B depends on the particular technology used: analog or digital beam forming, [Hansen09], [Johnson93]. The digital beam-former technology is currently more

favored as the number of connections needed to form the beams is determined by software rather than in the number of hardware fixed connections as in the analog beam-former case. The disadvantage is of course the bandwidth needed to process the signals to form the beams. Notice that all the beams are formed simultaneously rather than sequentially by electronically scanning the weight sets.
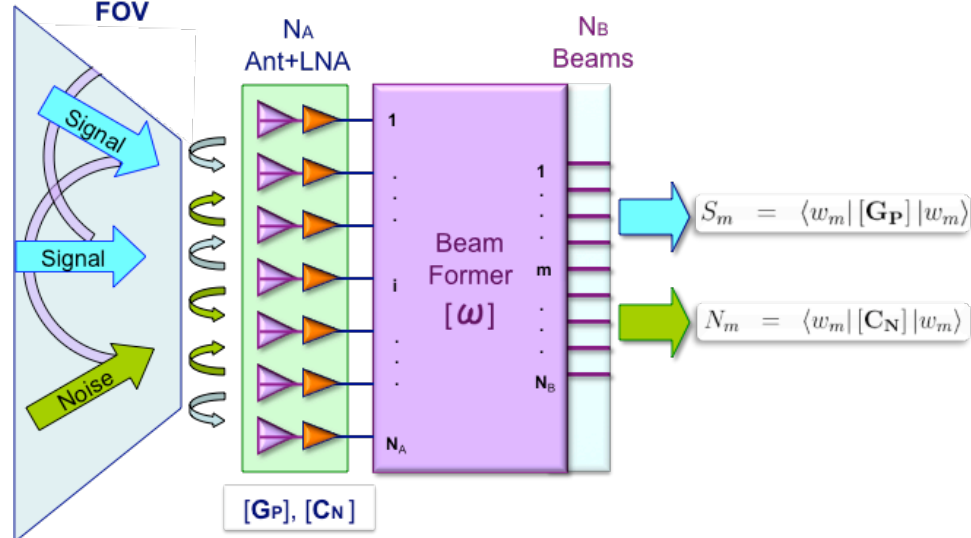

Figure 5. Basic operation of a focal phased array feed

The FOV of the PAF for astronomical operation is limited by the available FOV of the optics of the telescope in the focal plane as indicated in the figure. As the array is sensitive to both, the signal of interest and thermal noise, including self-generating noise coupled by neighboring antenna elements, the output of the beam former contains both, and calibration is needed to extract the signal. The weights ω_m then could be optimized to maximize sensitivity (S/N) or maximize antenna gain (Aeff), or FOV flatness, for example [Van Trees03].

Survey Speed and AO PAF

An important figure of merit, especially of large collecting aperture telescopes such AO is the survey speed: [Cordes09](here for steady sources),

$$\text{SVS} = N_b \, \Omega_b \, BW \, (A_{\text{eff}}/T_{\text{sys}})^2$$

N_b is the number of beams; Ω_b is the beam width of each. Therefore, the product, $N_b\Omega_b$ is the instantaneous FOV. *BW* is the instantaneous processing bandwidth and $(A_{\text{eff}}/T_{\text{sys}})$ the antenna sensitivity in m^2/K. As this factors in as square, AO has a great advantage with its 300 m diameter aperture compared with other telescopes, but also requires very good control of system temperatures. Table 1. Shows a survey speed comparison between Single pixel, ALFA and what we envision as a possible AO PAF instrument.

Table 1. Survey Speed Comparison

L-Band	N_b	Ω_b	BW	A_{eff}	T_{SYS}	A_{EFF}/T_{SYS}	SVS/ AO_{SVS}
		[deg²]	[MHz]	[m²]	[K]	[m²/K]	
AO	1	0.0028	300	32750	27	1213	1
ALFA	7	0.0028	300	32750	27	1213	7
AO FPA	40	0.0028	300	32750	35	936	23.8

We have used the equivalent of a 40 beams FOV and an estimated system temperature of 35K, which is feasible in the short term. With this, AO PAF is expected to have a factor of 3 to 4 in survey speed compared with ALFA and a factor of more than 20 when compared with a single pixel system.

AO PAF Feasibility Study

Three key aspects of this PAF technology are currently being assessed in the AO PAF feasibility study: the available FOV at AO, PAF cryogenics and PAF processing bandwidth. We are in the process of completing the first task, by measuring the AO's available FOV using a 19 element PAF from Brigham Young University [Warnick09]. The second aspect is PAF cryogenics that addresses the challenge of cryogenic design to achieve 35K of system temperature with a 120-element PAF and approximately 1.2 m in diameter. For that purpose, we are designing a smaller cryostat system for 7 dual polarized dipole elements that will operate at 15K at the LNA stage with the dipoles encapsulated in the vacuum environment. The main goal of this design is to demonstrate scalability up to 120 elements, with special emphasis in servicing, packaging and power consumption. At the same time, we are following closely also NRAO's efforts in the PAF cryogenics [Norrod10]; although, their approach only cools down the LNA with the dipoles left at room temperature. Finally the processing bandwidth, that we have chosen: 300 MHz is also the current standard bandwidth for digital beam forming pursued both by ASKAP (the Australian SKA pathfinder, CSIRO) and APERITIF, ASTRON, in the Netherlands.

Available AO FOV Experiment

As we mentioned, one important aspect of the feasibility study is to measure the size of AO FOV viewed by a phased array feed instead of single feed. In particular we are interested in determine the -1dB loss FOV area for AO with PAF's. This will untimely determine the number of elements and actual size of the array properly matched to that FOV. Ideally, this could be done simply by placing a large enough array in the focal plane of the AO optics, and form beams in different directions in the FOV and determine the area in the sky for which the losses are less than -1.0 dB. Since a large array is not available, instead, we used Brigham Young University's (BYU's) – BYU

was under contract to Cornell/NAIC to collaborate on the measurements - 19-dipole PAF, and by moving the PAF in the focal plane of the AO optics we produced the equivalent of a larger array. To move the BYU PAF we used a 3-degrees-of-freedom, electronically controlled, positioner arm mounted at the focal plane of the telescope optics (Figure 6).
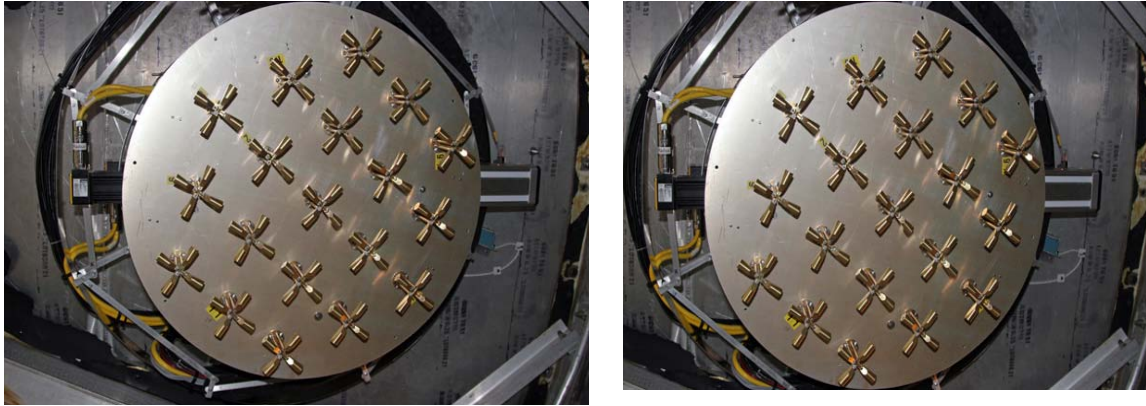

Figure 6. Left: work envelope of the positioner and 19-Element BYU's PAF system. Right: Complete system mounted in the telescope rotary floor for the measuring campaign.

Figure 6 (left), shows the work envelope of the positioner and BYU's 19 element PAF. The three degrees-of-freedom (azimuth, radial and focus position) allows positioning the 19-element PAF within a cylindrical volume of 1.7min diameter times 0.4 m in depth. Figure 6 (right), shows the BYU's 19-element PAF system mounted under the AO rotary floor for the measuring campaign.
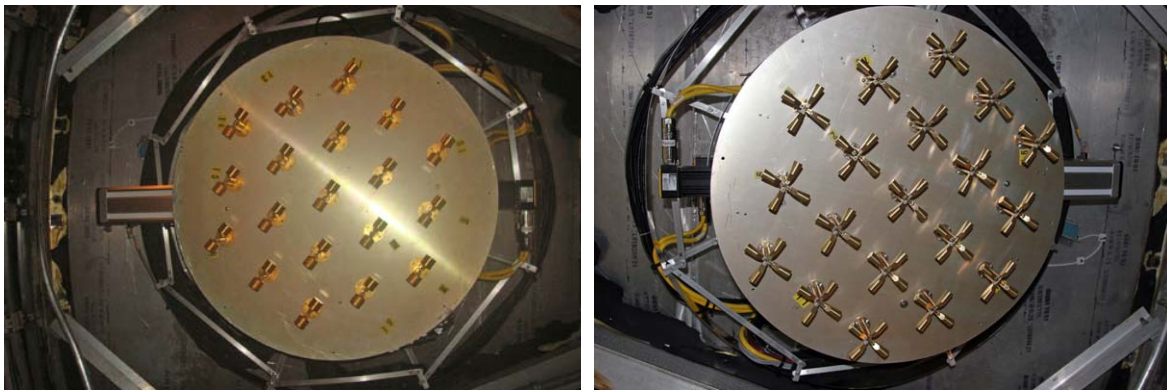

Figure 7. BUY 19-dipole Phased Array Feed, Left: Single Polarization. Right: Dual Pol

The 19-element PAF operates at 1.6 GHz and has a hexagonal layout (element separation=11.24cm), both for single and dual polarization, as shown in Figure 7 above. By placing the PAF on a hexagonal mosaic pattern, 19 elements at a time, over a pre-determined grid it is possible to mimic in first order a larger element array.

Before proceeding with the observing campaign, we made a series of simulations to have a better understanding of what to expect from the optics, to plan the observing runs, and interpret the measurement results. Figure 8, left, shows a mosaic layout in the focal plane (dipoles are out of the page), with seven non-overlapping positions (B0-B6), used for the simulations; on the right the figure shows the calculated sky foot print of the 133 (19x7) beams corresponding to these 7 positions, but with an artificially separation between beams in order to tell apart the individual beam patterns.

$$SVS = N_b \, \Omega_b \, BW \, (A_{eff}/T_{SYS})^2$$

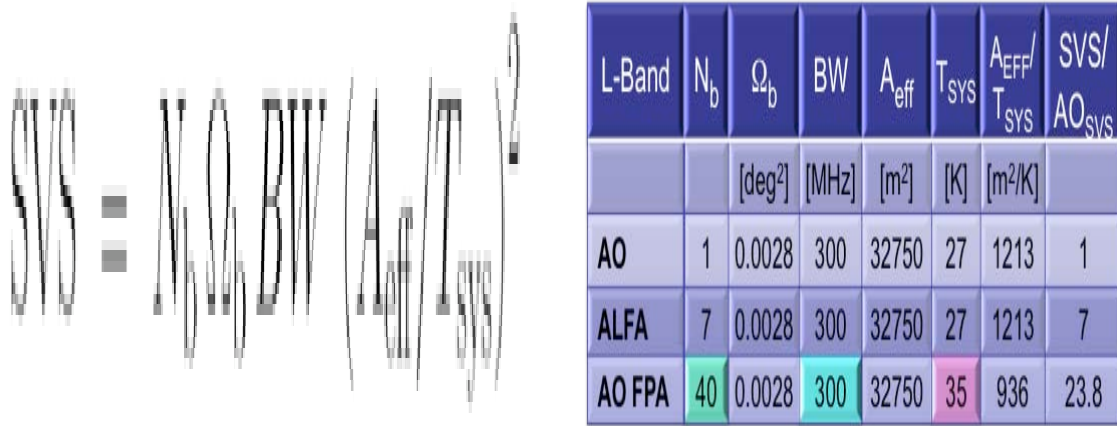| L-Band	N_b	Ω_b	BW	A_{eff}	T_{SYS}	A_{EFF}/T_{SYS}	SVS/AO_{SVS}
		[deg^2]	[MHz]	[m^2]	[K]	[m^2/K]	
AO	1	0.0028	300	32750	27	1213	1
ALFA	7	0.0028	300	32750	27	1213	7
AO FPA	40	0.0028	300	32750	35	936	23.8

Figure 8. Left: Mosaic B, corresponding to seven non-overlapping positions that fill-up the 1.2m diameter in the focal plane of the AO telescope. Right: Corresponding beam pattern sky foot prints with an artificial separation to visualize the individual beams.

Individual element sky-patterns, beyond the 4th hexagonal ring, show severe distortion, with large coma lobes and substantial gain degradation. In addition, there is a slight distortion in the overall final positions of the patterns in the FOV, due to the optics. This is the challenge that the PAF system should face.
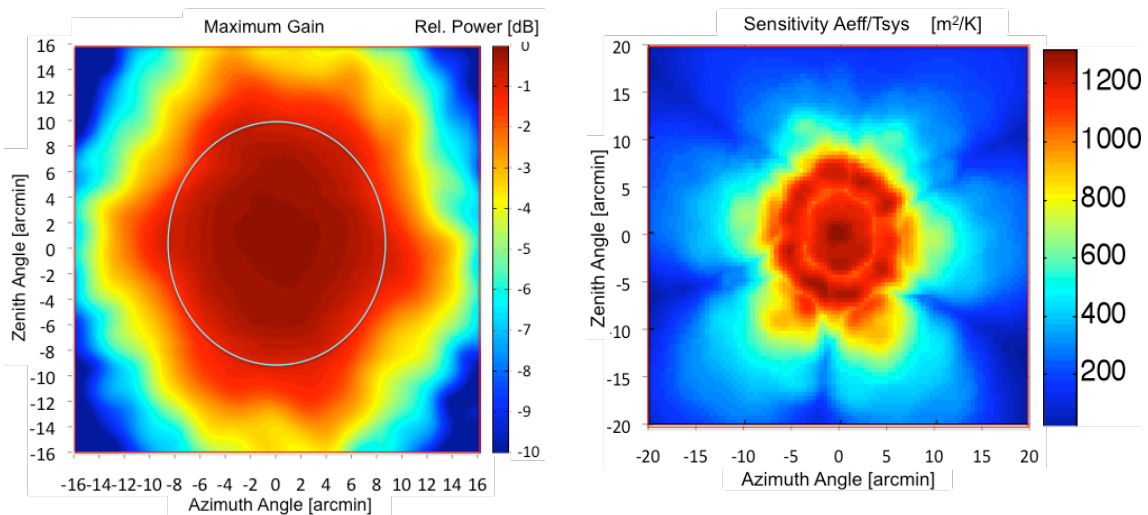
Figure 9. Left: Simulated FOV beam former optimized for maximum antenna gain. The ellipse corresponds to -1.0dB loss level. Right: simulated FOV optimized for

maximum sensitivity (Aeff/Tsys) for an assumed 15K LNA receiver temperature. As we mentioned earlier, it is possible to combine the different beams in the array to maximize either the overall antenna gain, or the sensitivity (Aeff/Tsys), in a given direction in the FOV; Figure 9 (left) shows an example of a calculated gain map in the FOV, with the beam former weights of the 133 beams optimized for maximum gain (maximum aperture efficiency). The ellipse indicates approximately the -1.0dB level. Figure 9 (right) shows the simulated FOV that could be obtained for maximum sensitivity (Aeff/Tsys) weighting instead assuming a LNA temperature of 15K.

Figure 10. BYU's 19-element single-pol PAF mounted under the rotary floor of AO for the FOV Experiment.

FOV Experiment:

For the AO FOV measurement campaign (Figure 10) we choose to have overlapping positions of the 19-element PAF, (See Figure 11). The first set of positions, circumscribed inside of a 1.0m diameter circle, is A0 to A6 (left of Figure 11). We also defined two other sets C1-C6 and D1-D6 shown in Figure 10 right.
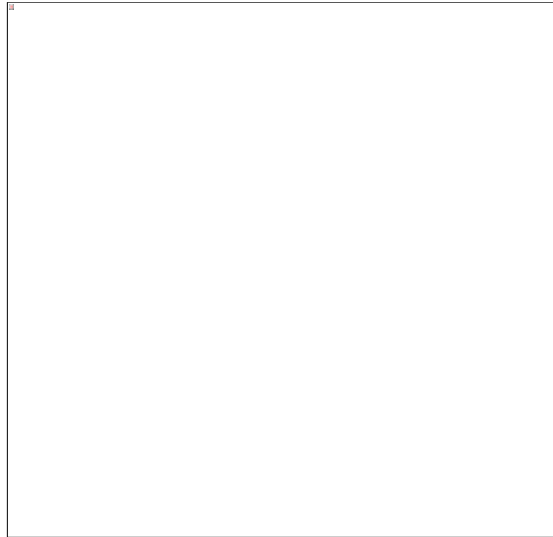
Figure 11. Overlapping positions A0-A6, left, and C's and D's used to mosaic the focal plane during the observing campaign.

The calibration procedure of the array is as follows, We moved the array to a given mosaic position in the focal plane, then the telescope is pointed such that a point source falls at the center element of the array, and then a calibration is set up centered in that position in the sky, and then, the telescope is pointed so that the point source moves though each calibration point in the grid. This is the "on" position, to extract the noise; the telescope is pointed to an "off" position to sample the blank field. The correlation matrices of the signal + noise and noise fields are then used to obtain the beam former weights. Coarse grids were 7x7; fine grids 15x15 and superfine grids 31x31. For a 31x31 superfine grid the calibration process takes approximately 2.5hours. The data is digitalized and process off-line as it is very computationally intensive.
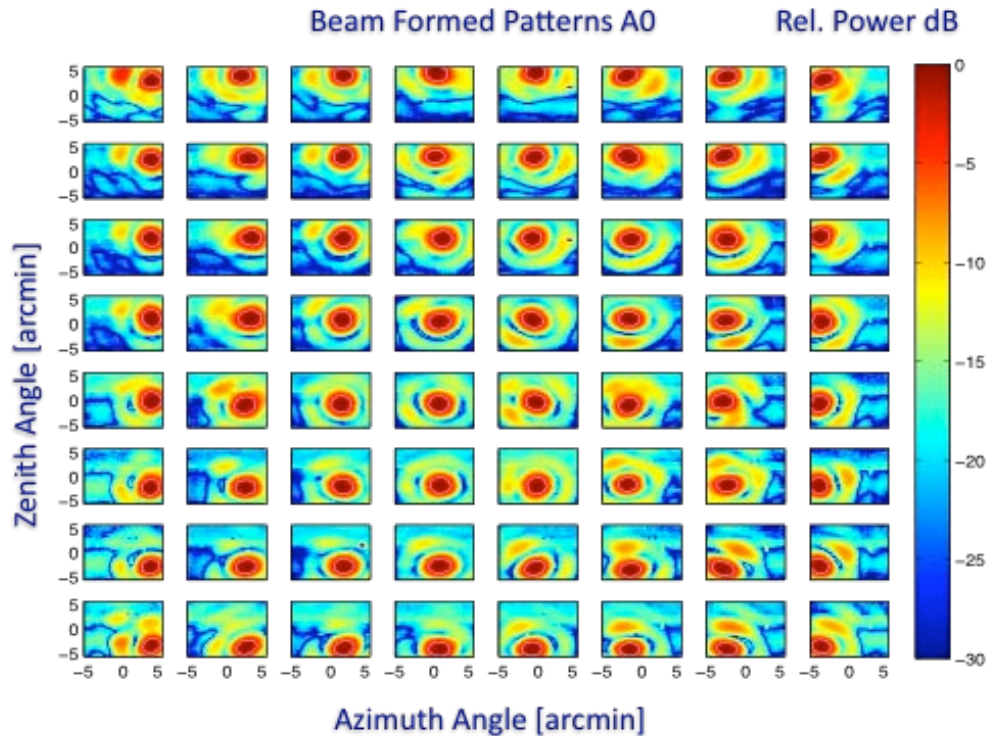
Figure 12. Beam formed pattern shapes for different directions in the FOV at the A0 position.

Figure 12 shows the beam formed pattern shapes for different directions in a 5x5 arc minutes^2 area in the FOV, corresponding to the array position A0 in the focal plane. Most of the beams have elliptical shape. The weights were optimized for maximum sensitivity (S/N), as this is achieved the shape of the first side lobe level varies.

Figure 13 shows the sensitivity (Aeff/Tsys) vs. focus variation, for the formed beam at two mosaic positions in the focal plane: A0 and A1. Also, it shows a comparison of the measured sensitivity using just the center dipole at each mosaic position. For a single dipole at the A0 position the peak in sensitivity is at approximately z=-8cm, whereas, for the A1 center dipole is close to z=0cm. In contrast, the beam formed has sensitivity is a factor 1.6 higher, with an approximately flat response for focus positions z varying from -10cm to 0 cm.
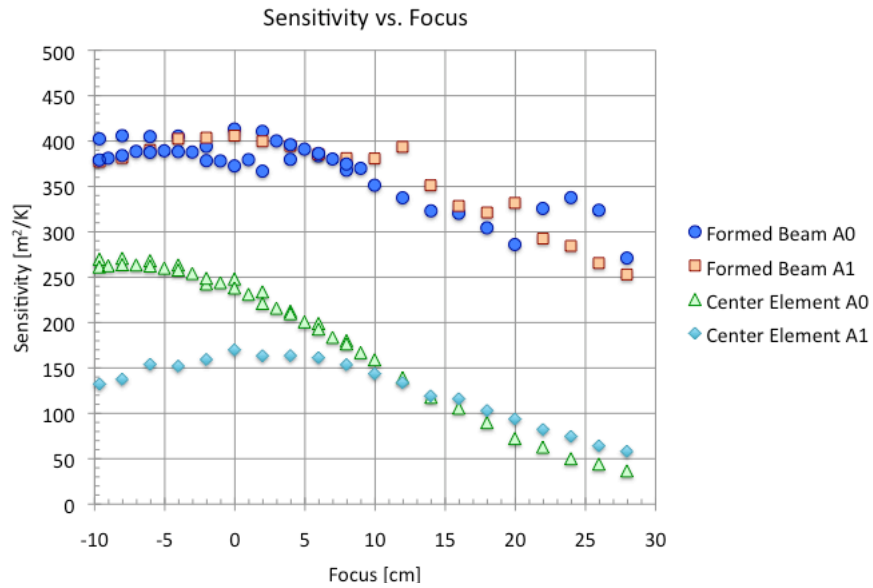
Figure 13. Sensitivity variation versus z-focus position of the array for the A0 and A1 configurations, and comparison between the center element sensitivity and the formed beam sensitivity.

Figure 14 shows the measured sensitivity (Aeff/Tsys) combined maps for different values of focus for the A0 to A6 mosaic positions. This is to investigate the location that maximizes available FOV, close to the exit pupil of the telescope optics. Although, the available FOV is larger at the exit pupil of the telescope, it does not yield the highest sensitivity. Therefore a tradeoff between sensitivity and size of FOV that has to be considered in astronomical use.
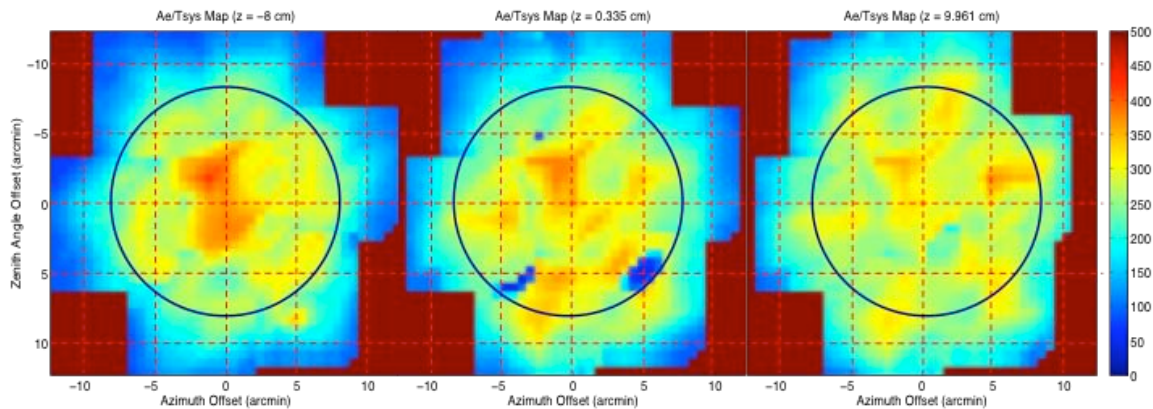

Figure 14. Measured Sensitivity maps for three different z-focus positions. Reference circle is 8-arcmin in radius.

The data processing of the AO FOV experiment is still under way, and further results are expected.

References

[Cordes09]   J.M. Cordes, "Survey Metrics", SKA Memo Series, No. 109, 2009

[Hansen09]   R. C. Hansen, *Phased Array Antennas.* John Wiley and Sons, 2nd Ed. Hoboken New Jersey, 2009.

[Johnson93]   D. H. Johnson and D. E. Dudgeon, *Array Signal Processing: Concepts and Techniques.* Prentice Hall, Englewood Cliffs, New Jersey, 1993.

 [Norrod10]   R. Norrod, "Cryogenic PAF Development, Progress Report". *International Workshop on Phased Array Antenna Systems for Radio Astronomy*, Brigham Young University, Provo, UT USA, May 3-5, 2010.

[Van Trees03] H.L. Van Trees, *Optimum Array Processing, Part IV of Detection, Estimation, and Modulation Theory. John* Wiley and Sons, New York, Ch. 6, 2002.

[Warnick09]   K.F. Warnick, B.D. Jeffs, J. Landon, J. Waldron, D. Jones, J.R. Fisher, and R. Norrod, "Beamforming and imaging with the BYU/NRAO L-band 19-element phased array feed". *13th International Symposium on Antenna Technology and Applied Electromagnetics and the Canadian Radio Sciences Meeting, Banff, AB. Canada, 15-18 Feb. 2009*